AIRFOIL STALL PENETRATION AT CONSTANT PITCH RATE AND HIGH REYNOLDS NUMBER

Peter F. Lorber and Franklin O. Carta
United Technologies Research Center
East Hartford, Conn.

MODEL WING IN WIND TUNNEL

The model wing consists of a set of fiberglass panels mounted on a steel spar that spans the 8 ft. test section of the UTRC Large Subsonic Wind Tunnel. The pitch angle of the model is set by hydraulic actuators attached to each end of the spar and controlled using a dual channel closed-loop system. This allows 1024 samples of each data channel to be acquired at identical positions during each cycle of the wing motion. The first use of this system was to measure surface pressures and flow conditions for a series of constant pitch rate ramps and sinusoidal oscillations at Mach numbers between 0.2 and 0.4, Reynolds numbers between 2 and 4×10^6, and pitch rates between $A = c\dot{\alpha}/2U = 0.001$ and 0.02.

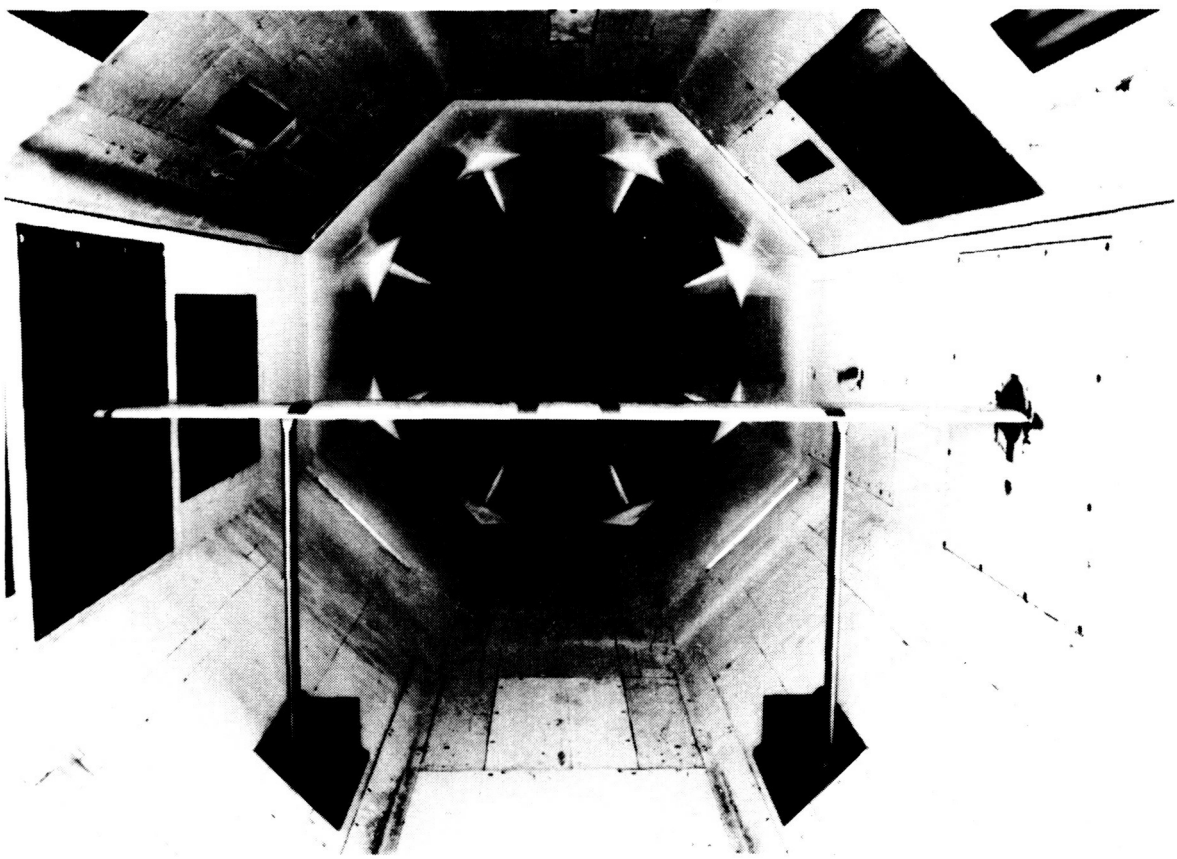

ORIGINAL PAGE
BLACK AND WHITE PHOTOGRAPH

AIRFOIL SECTION

A Sikorsky SSC-A09 airfoil with a 17.3 in. chord was used. This is a 9% thick supercritical section designed for low drag at high subsonic Mach numbers.

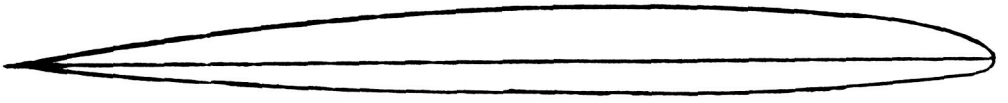

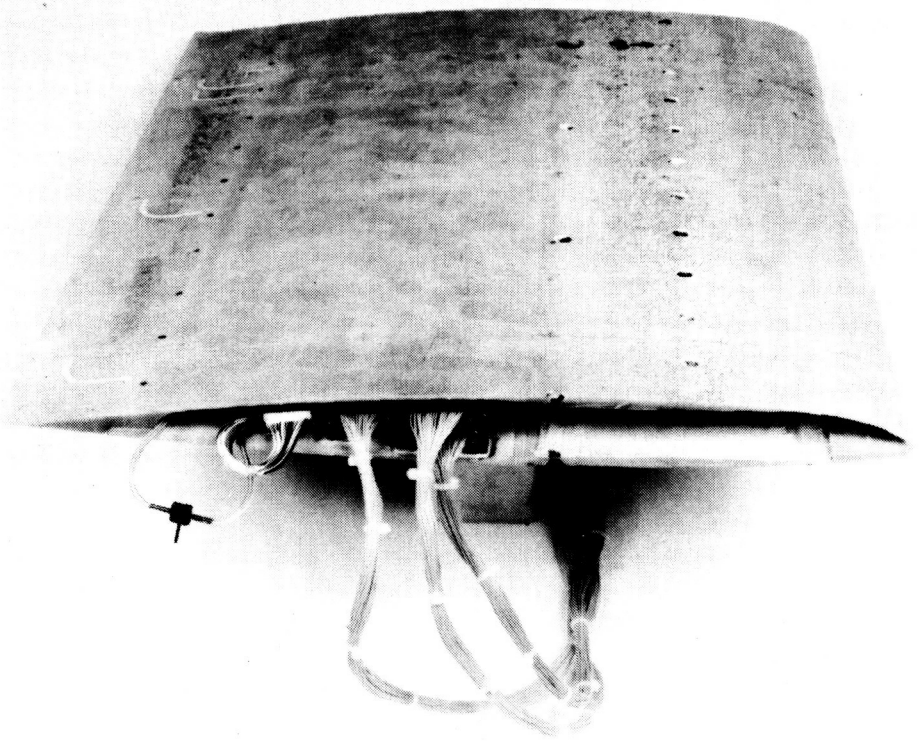

INSTRUMENTATION

The wing-mounted instrumentation consists of 72 miniature pressure transducers and 8 surface hot film gages. The pressure transducers are mounted inside the fiberglass skin and are connected to the surface by short pipettes. This technique provides a point measurement on a smooth surface contour. The primary chordwise pressure transducers are located in arrays of 18 on each surface, 0.5 chordlengths from the tunnel centerline, and 2.3 chordlengths from the side wall. The transducers are arranged in a segmented Gaussian array from x/c = 0.005 to x/c = 0.99. The other 36 transducers are located in additional arrays at 1.8 and 1.4 chordlengths from the wall, intended for use in future swept wing and finite tip experiments. The hot film gages are located in an array parallel to the primary pressure array, from x/c = 0.026 to x/c = 0.88. Detailed calibrations over both pressure and temperature ranges make it possible to measure both mean and unsteady pressures to within 1% of the calibration range. An interactive data system is used to acquire single samples of time histories, or to obtain an ensemble average of the time histories, based on 20 cycles of the motion. These data are digitized, converted to pressure coefficient, and stored on magnetic tape.

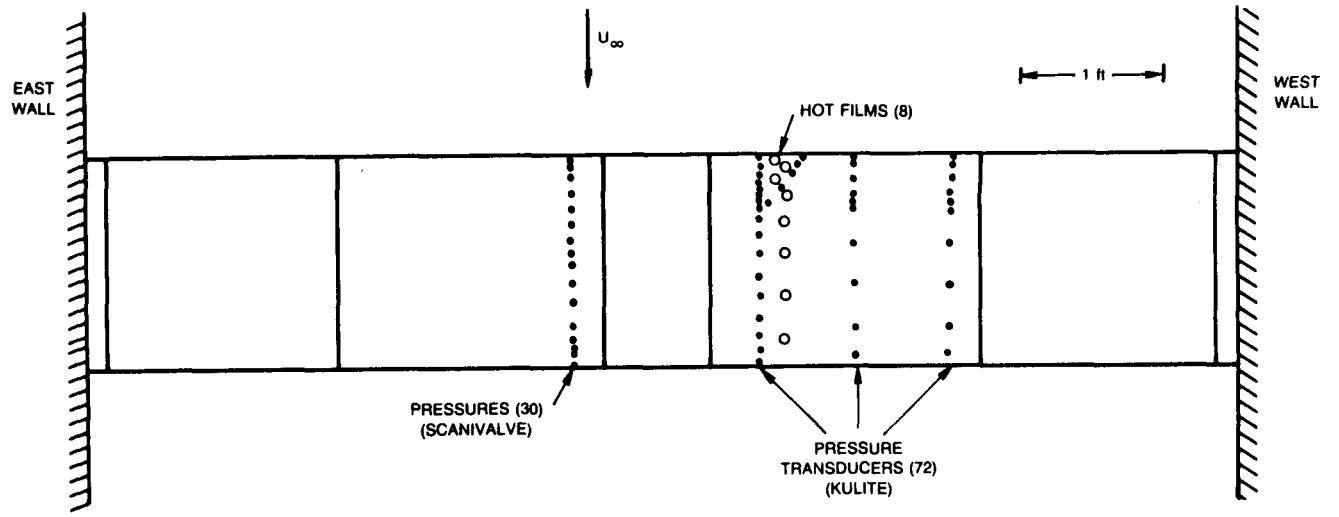

TEST CONDITIONS

Unsteady data were acquired for 36 constant pitch rate ramps and 9 sinusoidal oscillations, as shown in the table. The maximum pitch rate of 360 deg/sec occurred at A = 0.02 and M = 0.2, and the minimum of 18 deg/sec at A = 0.001. The maximum rate is lower than the maximum reached in many smaller scale experiments (Refs. 1-5), but is larger than that for both the "typical" (A = 0.001) and "minimum time" (A = 0.0044) maneuvers described in Ref. 6. The wing angle of attack was limited by the support system to a maximum of 30 deg, which was less than the maximum obtained in the smaller scale tests, but sufficient to include all of the primary stall-related events at the pitch rates used.

STEADY

$M = 0.2, \quad -5° \leq \alpha \leq 28°$
$M = 0.4, \quad 0° \leq \alpha \leq 20°$

UNSTEADY RAMPS

$A = C\dot{\alpha}/2U$

M	α—RANGE	.001	.0025	.005	.010	.020
0.2	0°→10°	x	x	x	x	
	0°→20°	x	x	x	x	
	0°→30°	x	x	x	x	x
	10°→20°	x	x	x	x	
	12°→22°	x		x	x	
	14°→24°	x		x	x	
	20°→30°	x	x	x	x	
	20°→10°	x			x	
	30°→ 0°	x		x		
0.3	0°→20°			x		
	0°→30°				x	
0.4	0°→10°	x		x		
	0°→20°	x	x	x	x	
	20°→ 0°				x	

(40 RAMPS)

UNSTEADY OSCILLATIONS

$k = C\omega/2U$

M	α	.025	.050	.100
0.2	$5° + 5°\sin\omega t$	x		
	$10° + 10°\sin\omega t$	x	x	x
	$20° + 10°\sin\omega t$	x	x	x
0.3	$9° + 8°\sin\omega t$		x	
	$12° + 8°\sin\omega t$			x

(9 SINUSOIDS)

The steady pressure distributions have a strong leading edge suction peak prior to stall. Maximum suction occurs at α = 13 deg and reaches values of C_p = -8.2 at M = 0.2, and C_p = -5.2 at M = 0.4. The sonic pressure coefficient at M = 0.4 is -3.7, so a small supersonic zone exists at the leading edge, terminated in a shock near x/c = 0.03. The compressibility effects associated with this zone create the lift curve differences seen earlier.

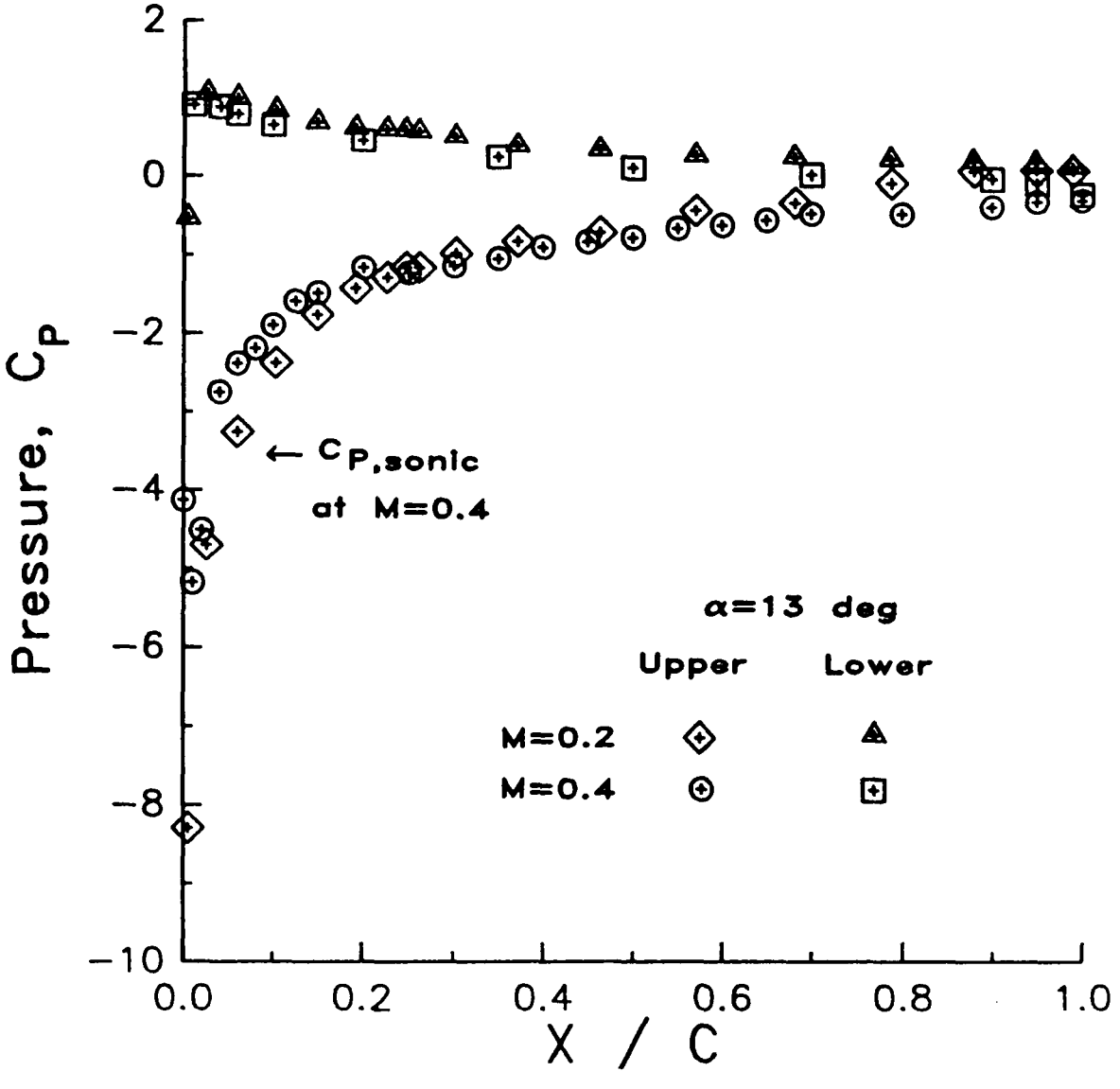

STEADY LIFT FOR M = 0.2, 0.4

Steady pressure data acquired at M = 0.2 and 0.4 were integrated to yield the lift curves shown in the Figure. At M = 0.2 max C_L of 1.4 is reached at α = 14 deg, and is followed by a rapid drop to a C_L of 0.9 at α = 17 deg. Increasing M to 0.4 reduces max C_L to 1.2 and flattens the stall.

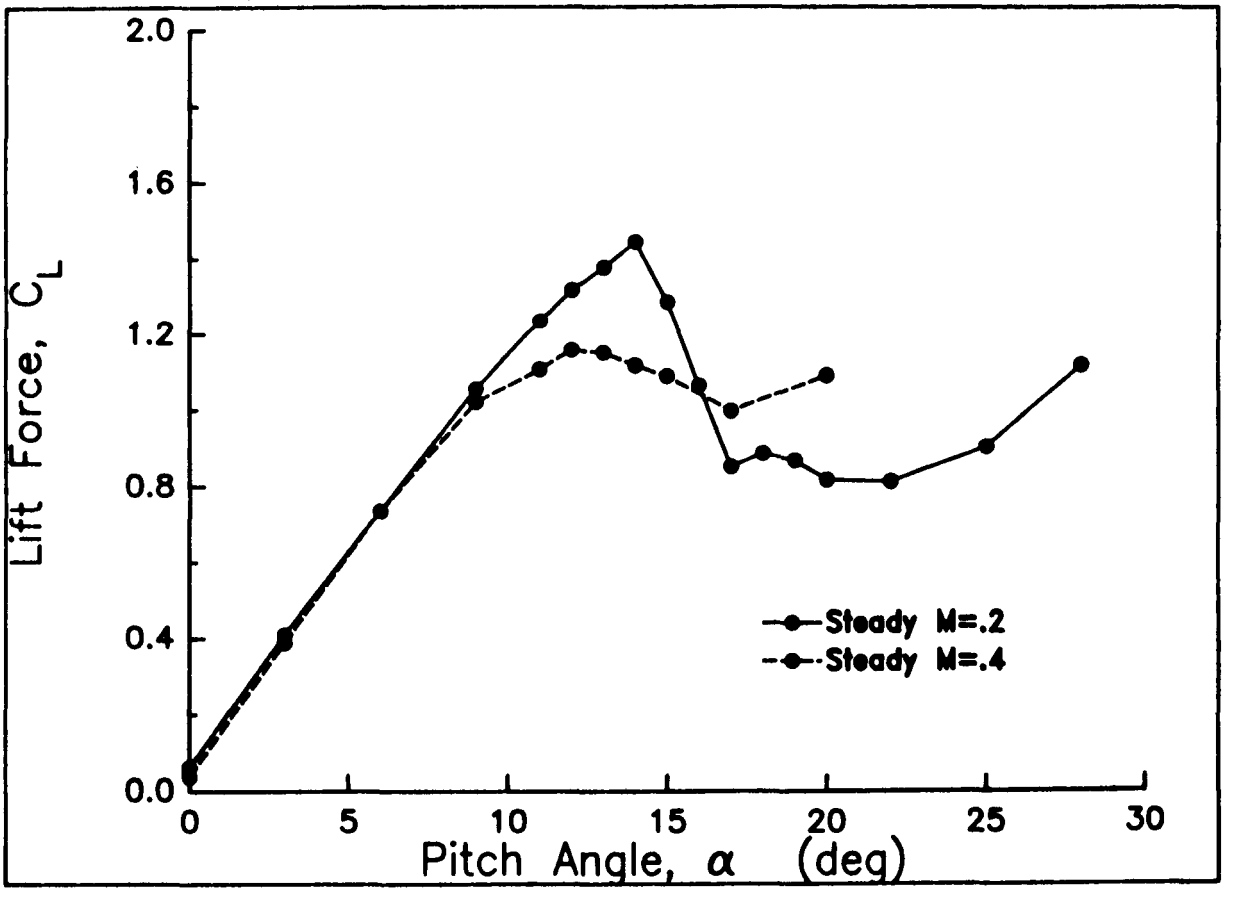

RAMP TIME HISTORIES

Airfoil motion for a ramp consists of an initial delay of several seconds at the minimum angle, a constant rate increase to the maximum angle, a second delay at the maximum angle, and a return to the initial condition. Data are acquired only during a small portion, T, of this cycle. Time histories of the pitch angle during the data acquisition period are shown in the figure for several 0 to 30 deg ramps at M = 0.2. The ramp begins at nondimensional time, τ = t/T, of 0.125 and ends at τ = 0.625. The pitch increase is quite linear with time and has sharp corners for A < 0.005. At higher pitch rates the damping of the hydraulic system rounds the corners, but still maintains a nearly linear pitch rate near stall.

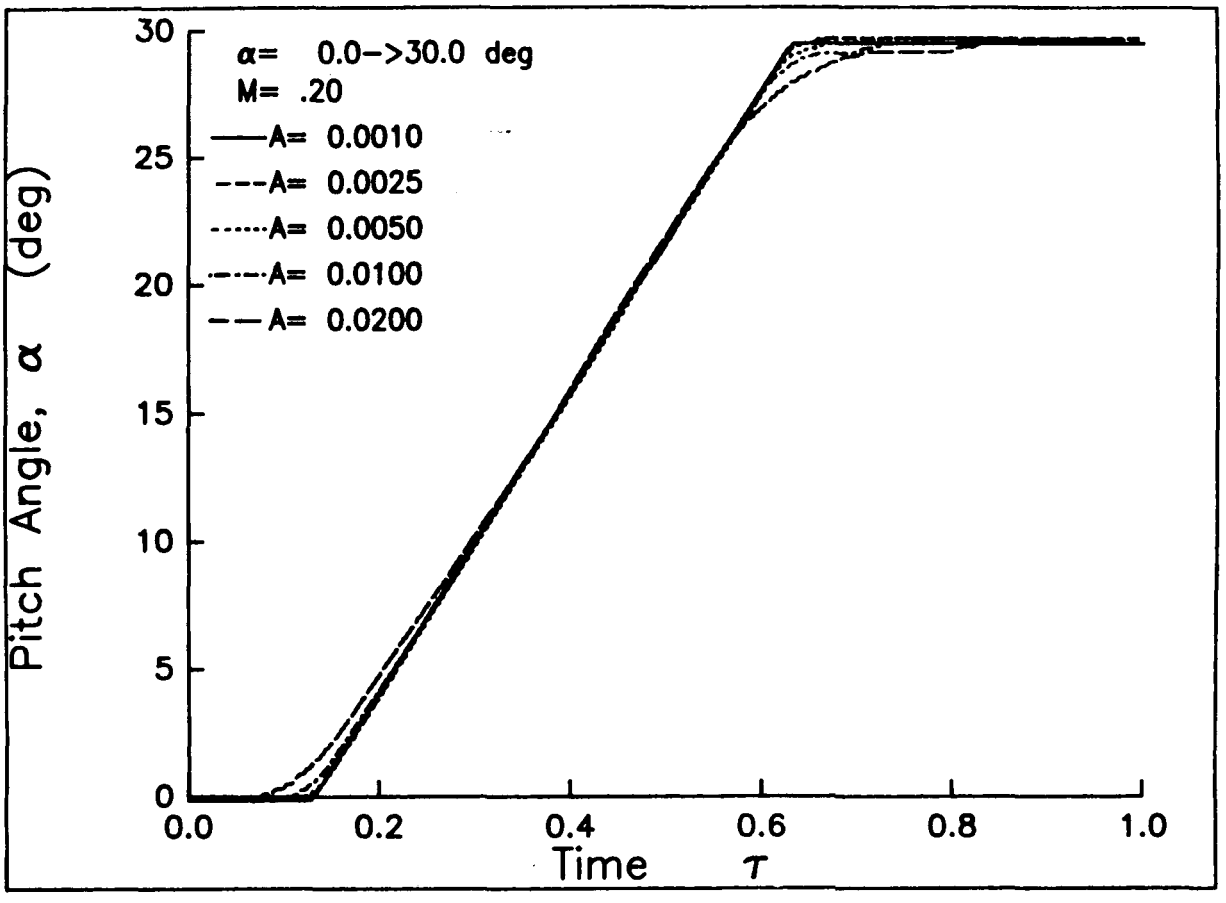

UNSTEADY PRESSURES, UPPER SURFACE

Ensemble averaged upper surface pressure time histories for 11 of the 18 measurement stations are shown for a 0 to 30 deg constant pitch rate ramp at A = 0.005, M = 0.2. The ordinate scale on the lower left refers absolutely to the x/c = 0.005 curve, and all other curves are vertically offset by ΔC_p = 1.0. Each of these curves is referenced to its own origin (upper left scale). The pressure responds smoothly to the imposed pitch angle until maximum suction is reached at τ = 0.4 (α = 15.5 deg) at letter A. Peak suction at x/c = 0.005 is C_p = -12.5, corresponding to a local Mach number of 0.84. The rapid local increase in suction associated with passage of the vortex (letter B) is only observed for x/c > 0.1, implying that the vortex forms ahead of this position and travels downstream thereafter. The vortex pressure propagates along the chord at 0.16U, and reaches the trailing edge at τ = 0.45. For τ> 0.50 the upper surface separation is massive and the pressures are virtually invariant in both time and position (letter C). All events are completed well before the ramp ends at τ = 0.625.

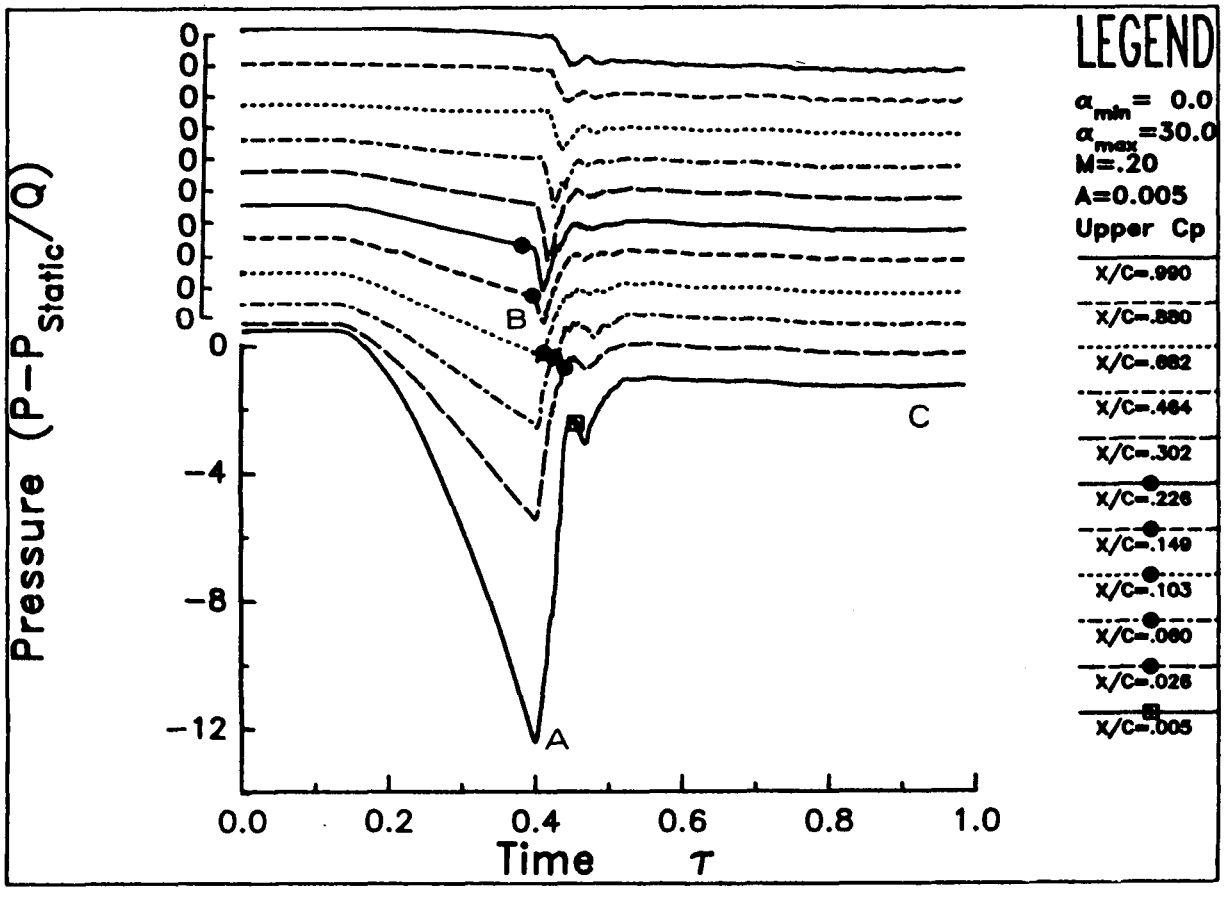

UNSTEADY PRESSURES, LOWER SURFACE

The lower surface does not separate, and responds primarily to the migration of the stagnation point near the leading edge (from motion initiation at $\tau = 0.125$ to $\tau = 0.42$), and to the upper surface massive stall near the trailing edge (letter A), where the pressure is required by continuity to match that on the upper surface. In addition, a periodic oscillation in these ensemble averaged pressures is detected near the lower surface trailing edge (letter B). The oscillation frequency of 62Hz is very close to the 65Hz frequency calculated for the vonKarman vortex street shed by a circular cylinder having a diameter, D, equal to the vertical projection of the airfoil chord, c sin α. From Ref. 7, a cylinder will generate a vortex street at a Strouhal number, Df/U, of 0.21 for Reynolds Numbers less than 10^6 and at fD/U = 0.27 for Re > 3×10^6. No regular vortex street is formed when the Reynolds number is between these limits. In the present case the Reynolds number of the cylinder is equivalent in projected area to the airfoil at M = 0.2 and α = 30 deg is 10^6, near the boundary where periodic oscillations should cease.

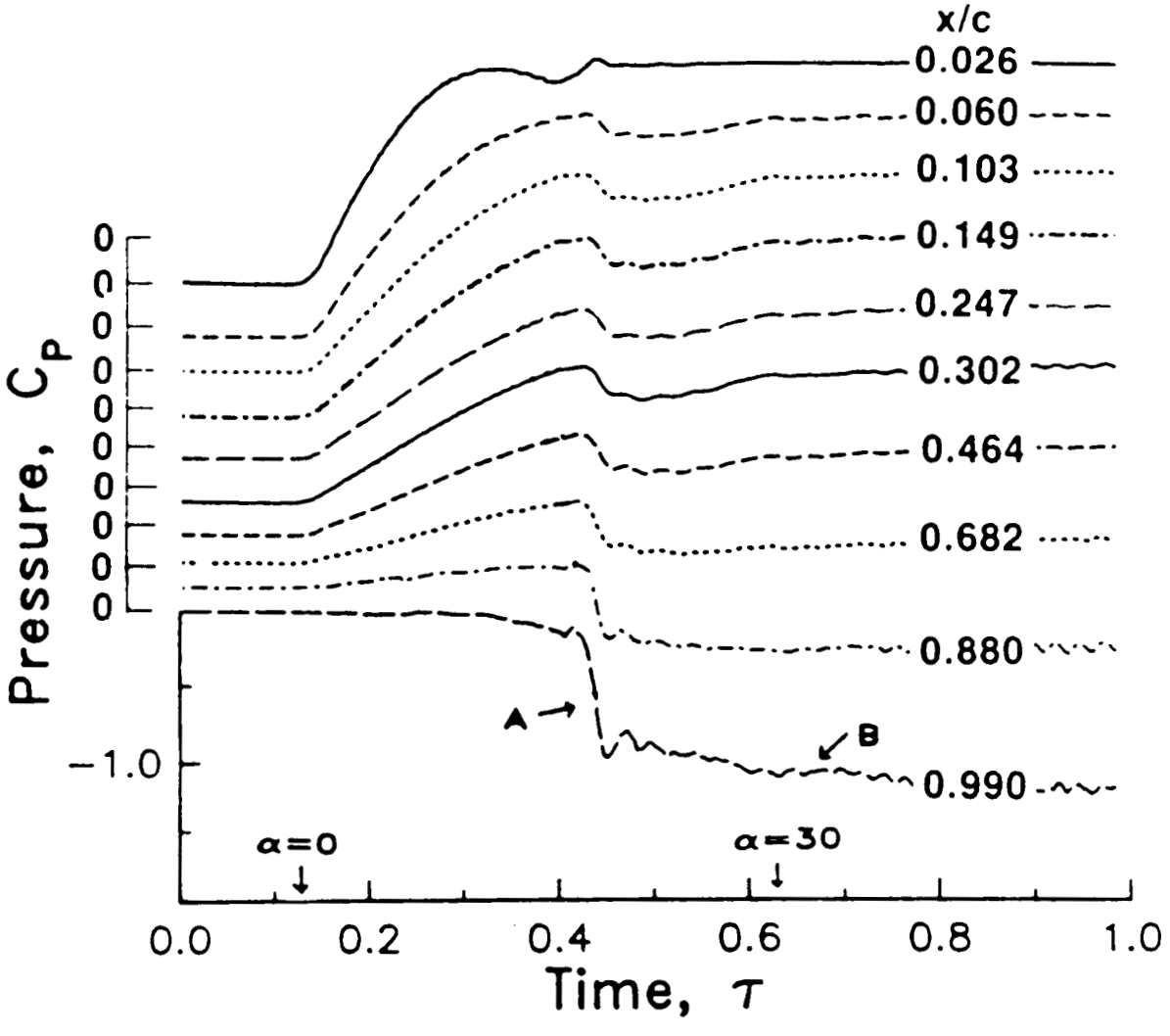

INDIVIDUAL RECORDS, LOWER SURFACE

A larger post-stall oscillation amplitude is found for individual records of the motion than for the ensemble average. The top time history in this figure is the ensemble averaged trailing edge plot from the previous figure, and the remaining curves are a set of (nonconsecutive) individual records at the same location and for the same set of flow conditions. Each curve is offset vertically by $C_p = 0.5$. The oscillations have the same frequency and a similar maximum amplitude during each record, but they are not well correlated in phase. The resulting cancellation reduces the ensemble averaged amplitude. A separate oscillation at a lower frequency is often present immediately following the passage of the stall vortex at $\tau = 0.45$ (letter A), and may result from secondary stall vortices.

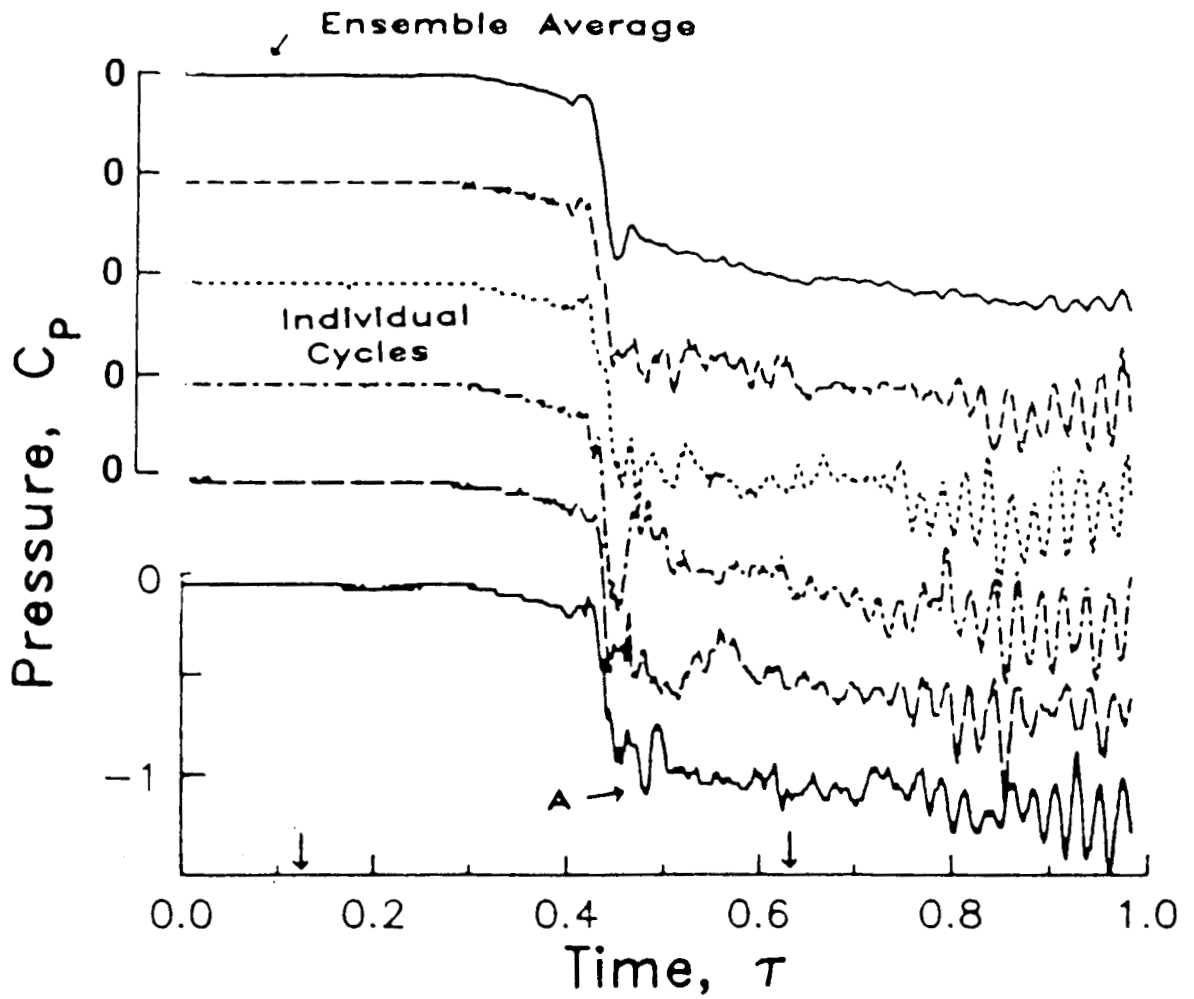

HOT FILM TIME HISTORIES

Hot film gages provide additional information on the surface flow conditions, as shown by the six time histories in this figure. The data are self-scaled, so each varies over one unit. As indicated on the leading edge trace, the boundary layer is initially laminar at the first two stations, goes through transition, becomes turbulent, and eventually becomes separated. From x/c = 0.192 and aft the flow is always either turbulent, or separated, and is never laminar. Ahead of the stall vortex release point (x/c = 0.1) the heat transfer drops when the boundary layer separates at τ = 0.4. Downstream of the release point the heat transfer drops slightly at separation but then rises rapidly as the high velocities induced by the stall vortex pass each gage. There is excellent agreement between the times of separation as measured by the hot film gages and by the adjacent pressure transducers.

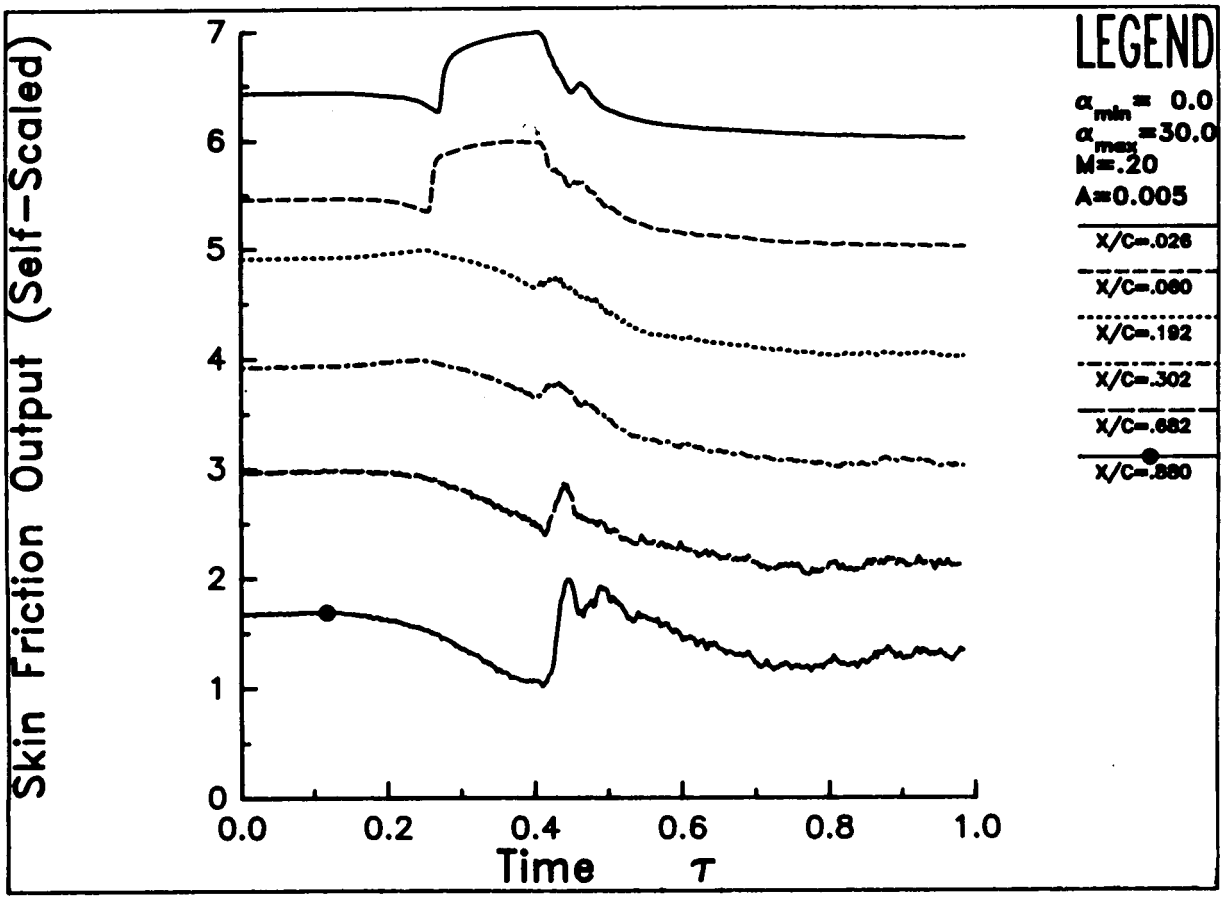

UNSTEADY PRESSURE, UPPER SURFACE, MAX PITCH RATE

At the maximum pitch rate of A = 0.02 the upper surface pressure time histories are qualitatively similar to the lower pitch rate results prior to stall, but are significantly different after stall. The unsteady increments to the airloads are strongly influenced by the strength of the stall vortex, which may be estimated by measuring the local change in C_p at some point along the chord downstream of the vortex release point, say at x/c = 0.302. This increment increases from ΔC_p = 1.0 at A = 0.001 (not shown here) to ΔC_p = 1.5 at A = 0.005 and to ΔC_p = 2.5 at A = 0.020 (below).

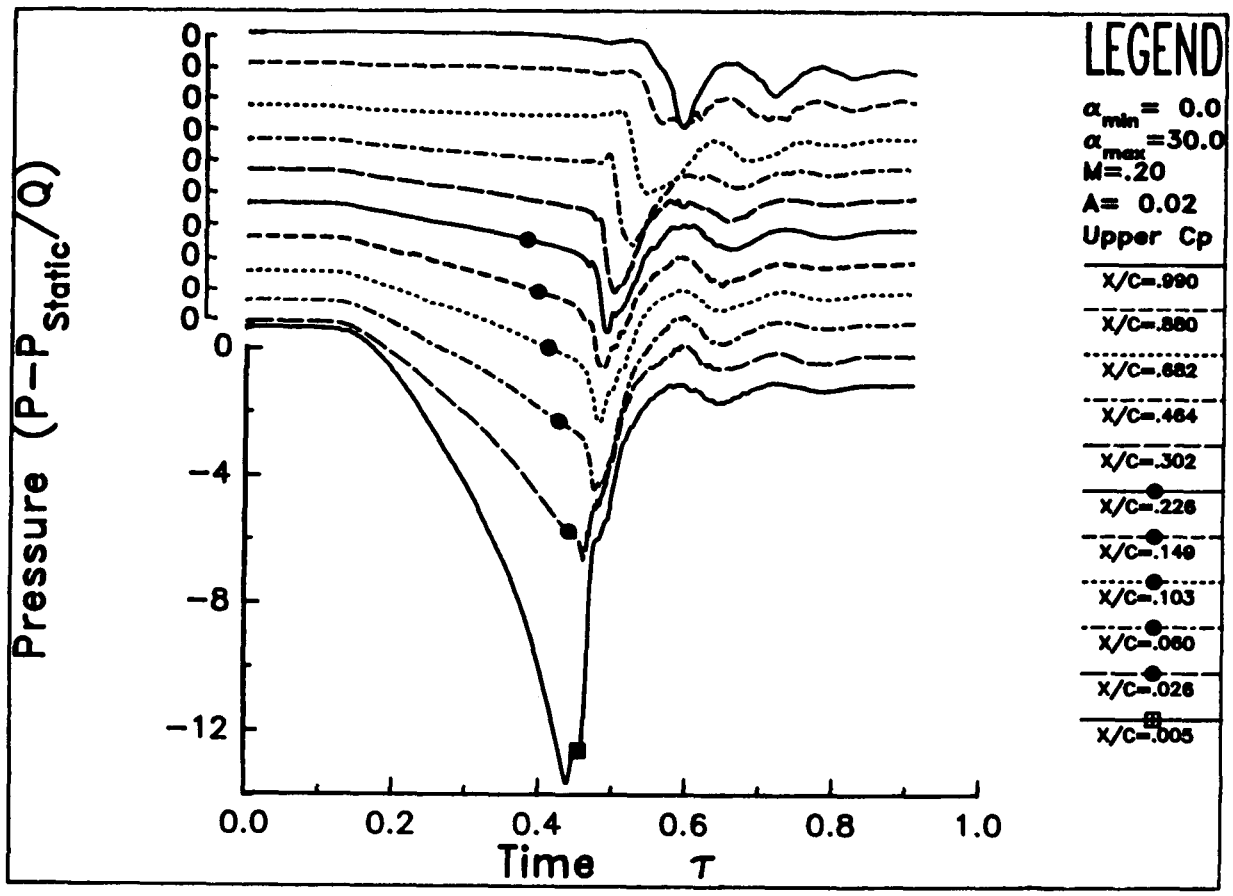

VORTEX PROPAGATION TRACES

The vortex propagation speed along the airfoil may be estimated using the times of minimum pressure at each transducer. These points are plotted below for 5 pitch rates. The region of constant vortex speed generally begins near x/c = 0.10 and ends between x/c = 0.80 and 0.90, and the speed in this region increases approximately linearly with pitch rates, from 0.13U at A = 0.001 to 0.33U at A = 0.020. These results are consistent with those of previous investigations (Ref. 8 for sinusoidal motions).

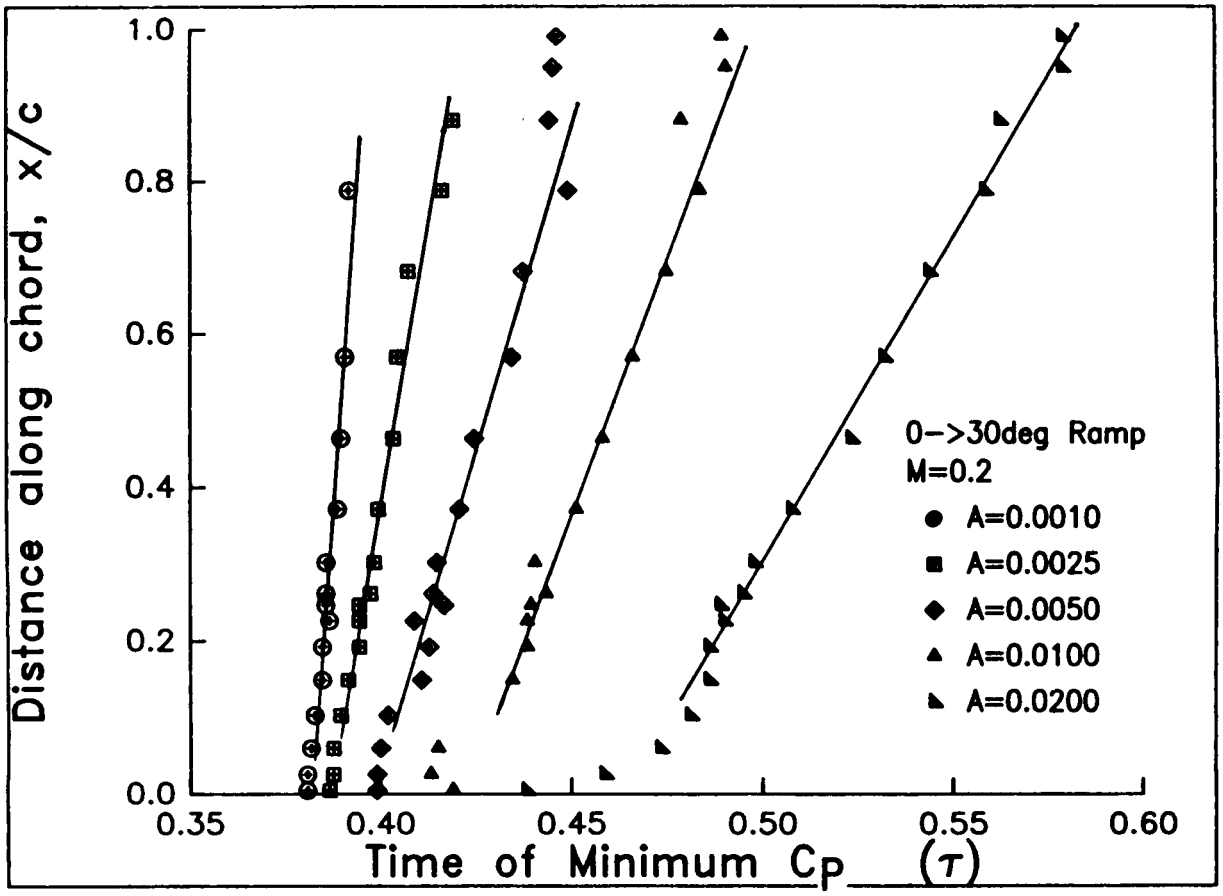

Integrated lift, pressure drag, and pitching moment (parts a, b, c) exhibit characteristic behavior with increasing pitch rate: (1) Before the stall vortex is formed, increasing pitch rate decreases the lift slope, decreases pitching moment, and increases drag. The lift slope effect agrees with the results of Ref. 2 at lower Reynolds number. (2) There is a rapid buildup of lift as the leading edge vortex forms. The unsteady increment added to the quasi-steady lift increases from ΔC_L = 0.4 at A = 0.001 to 1.1 at A = 0.020. (2) The pressure drag increases smoothly before stall, rises and falls rapidly as the stall vortex travels over the chord, then increases slowly as the pitching of the airfoil rotates the aerodynamic force vector. (4) The pitching moment in attached flow becomes more negative at higher pitch rate, following the prediction of thin airfoil theory (cf. Eq. 4-171 in Ref. 9). (5) The peak negative C_M after stall increases with pitch rate, from C_M = 0.22 at A = 0.001 to -0.52 at A = 0.020.

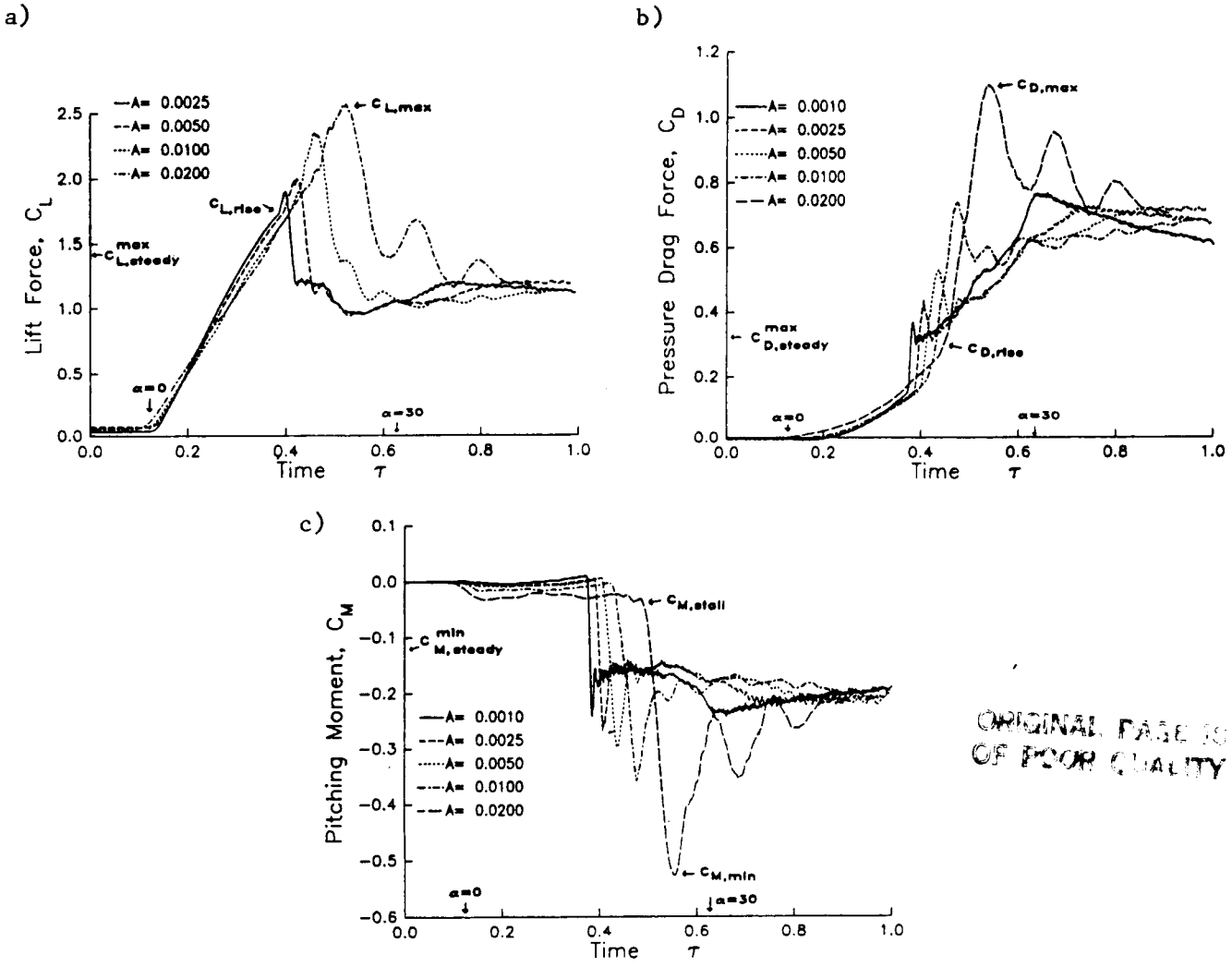

SEQUENCE OF STALL EVENTS

The sequence of stall events is systematic and each appears to be linear with pitch rate. First the stall vortex forms and C_L and C_D start to rise. Moment stall occurs when the vortex is released. Maximum C_L occurs as the vortex travels downstream along the chord, and when the vortex reaches the trailing edge, the minimum C_M and maximum C_D are obtained. At these pitch rates the angle when moment stall occurs increases approximately linearly with A, in agreement with results for a sinusoid at similar peak pitch rates (Ref. 8). This does not agree with the square root correlation postulated by Gormont (Ref. 10).

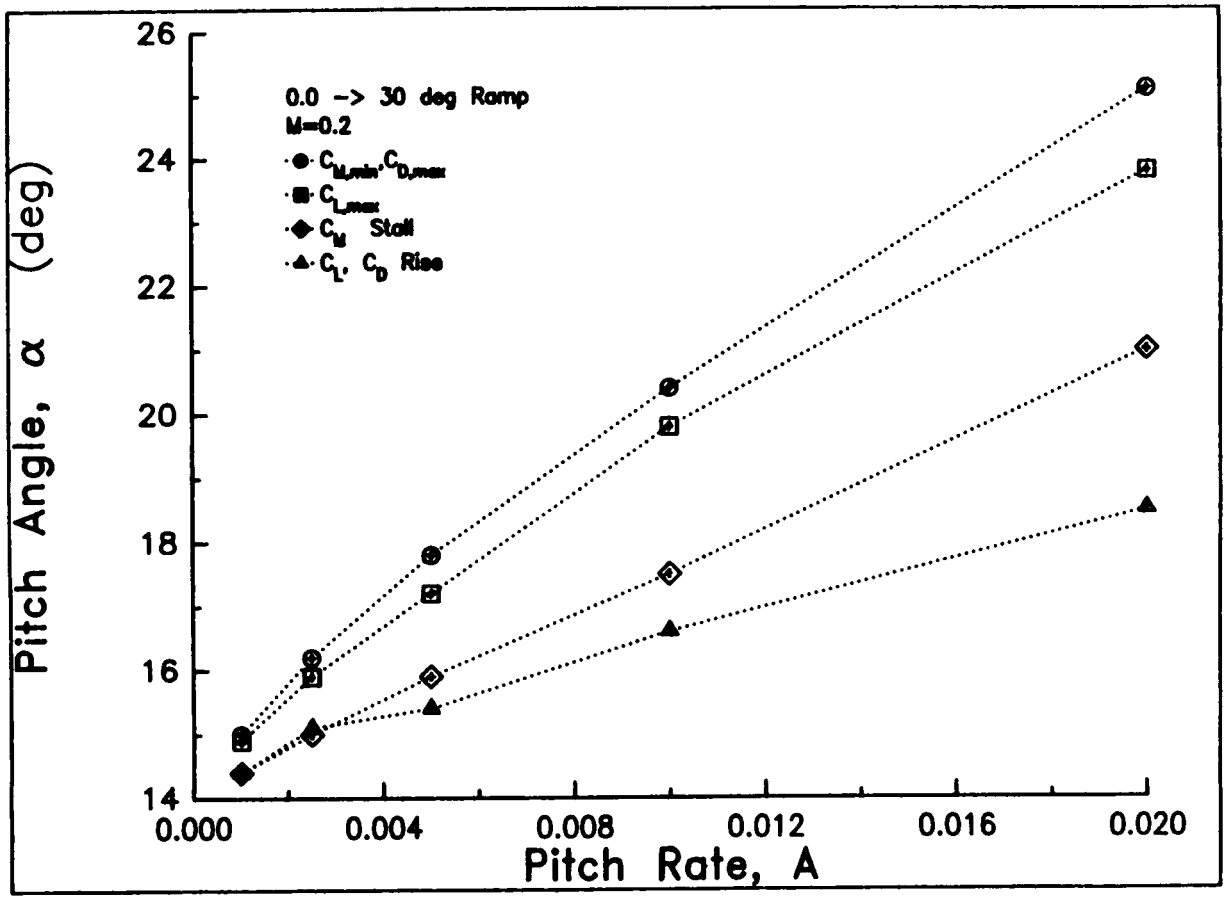

UNSTEADY PRESSURES, UPPER SURFACE, MAX MACH NO.

A supersonic zone at the leading edge has a profound effect on chordwise pressures at freestream Mach number M = 0.4. The time histories for this 0 to 20 deg ramp at A = 0.005 are not shifted vertically and the ordinate is an absolute measure for all curves. At x/c = 0.005 the flow becomes supersonic at τ = 0.34 (α = 7.6 deg) and reaches a peak local Mach number of 1.3 at τ = 0.45 (α = 10.6 deg). The sharp rise and fall of the pressure at x/c = 0.026 (letter A) is caused by the movement of the shock downstream past this station at τ = 0.40 and back upstream at τ = 0.46. A distinct stall vortex is released at τ = 0.46 and x/c = 0.060, just downstream of the shock (letter B). Several of the vortex characteristics differ from those at M = 0.2: (1) the release point is at x/c = 0.060 instead of 0.10; (2) the vortex speed is approximately 10% less than the speed at M = 0.2; (3) the strength of the vortex is reduced by approximately 50%; and (4) the pressure signature of the vortex is not observed downstream of x/c = 0.57. In addition, no clearly defined oscillations are present after stall at M = 0.4. The Reynolds number of the equivalent bluff body is 1.4×10^6 for this case, above the maximum of 1×10^6 for a stable vortex street (Ref. 7).

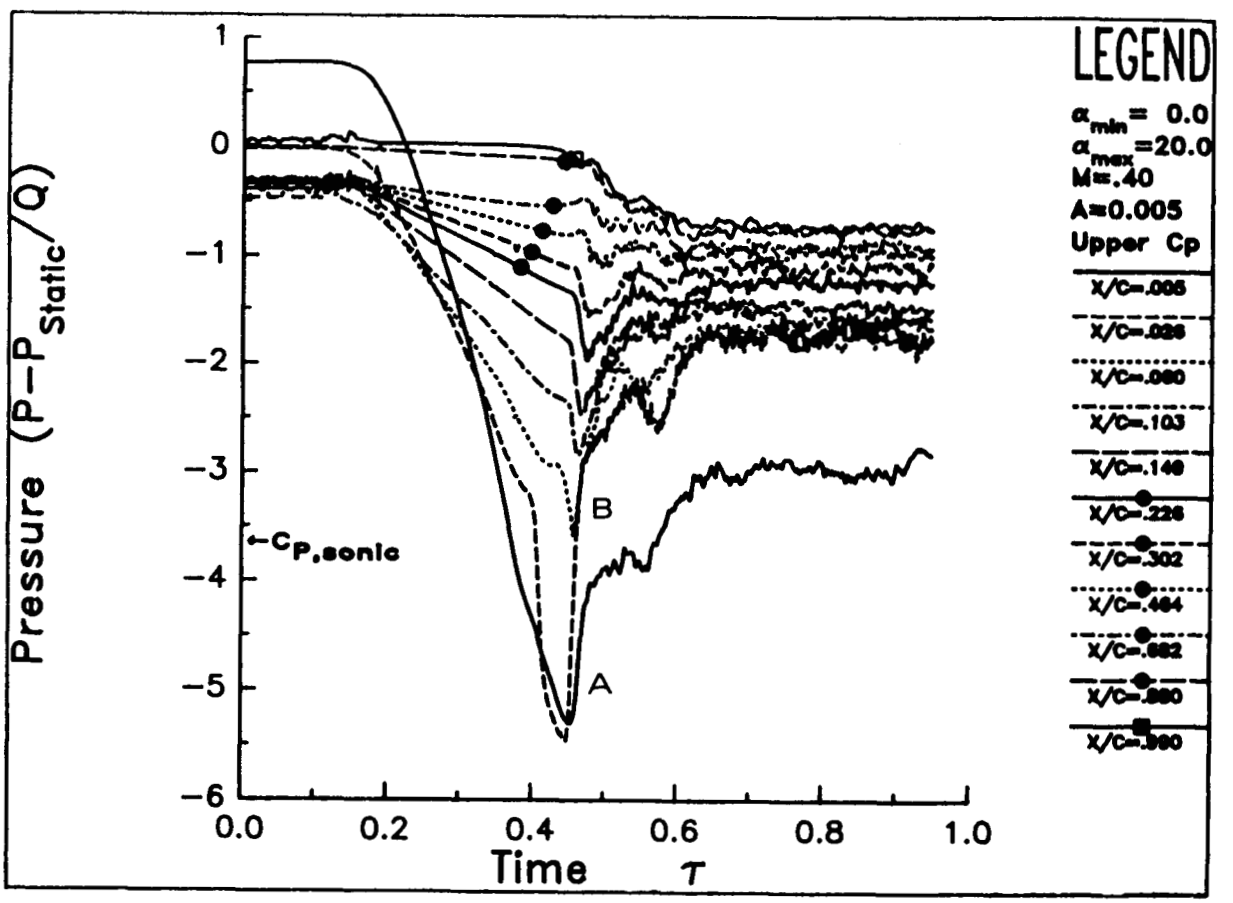

COMPRESSIBILITY EFFECT ON UNSTEADY LIFT

Increasing the Mach number also has a strong effect on the integrated loads. The vortex-induced peak in C_L diminishes markedly as M varies from 0.2 to 0.4, and its position retreats from approximately α = 16 deg to 12 deg. This suggests that compressibility prevents the development of the extremely strong suction peak seen at M = 0.2, and therefore reduces the strength of the stall vortex.

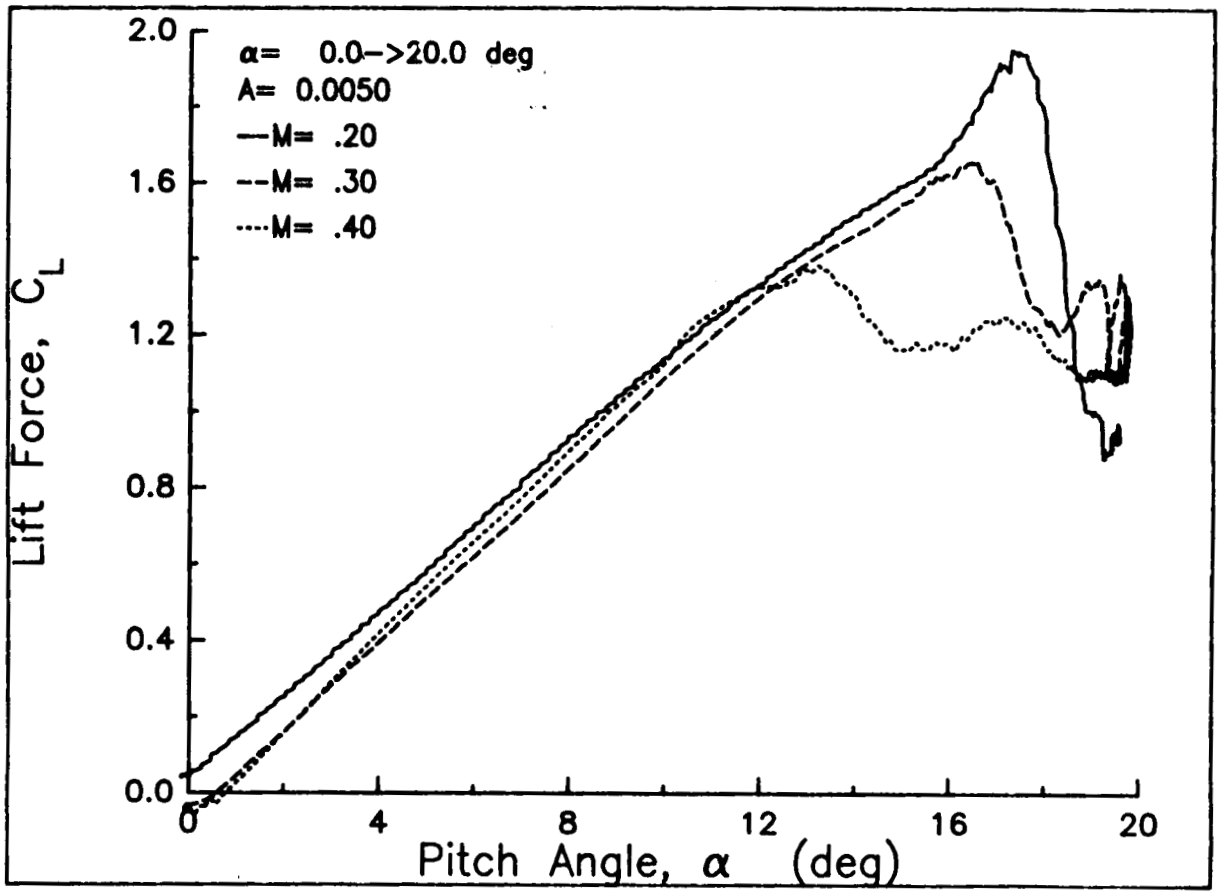

UNSTEADY PRESSURES, UPPER SURFACE, SINUSOID

Sinusoidal motion differs from ramp motion in two important aspects: in a sinusoid the airfoil does not start from a steady-state condition, and the pitch rate is constantly changing. Nonetheless, there are many qualitative similarities between the responses to the two motions. For the upper surface time histories shown here (α = 20 - 10 cos ωt at M = 0.2 and k = 0.05) the motion begins at τ = 0.0, reaches maximum pitch angle at τ = 0.50, and returns to the minimum value at τ = 1.0. Each time history here is offset vertically by ΔC_p = 1.0. The characteristics are similar to the constant pitch rate results shown earlier for A = 0.005, which is comparable to the instantaneous sinusoidal pitch rate at stall of A = 0.008.

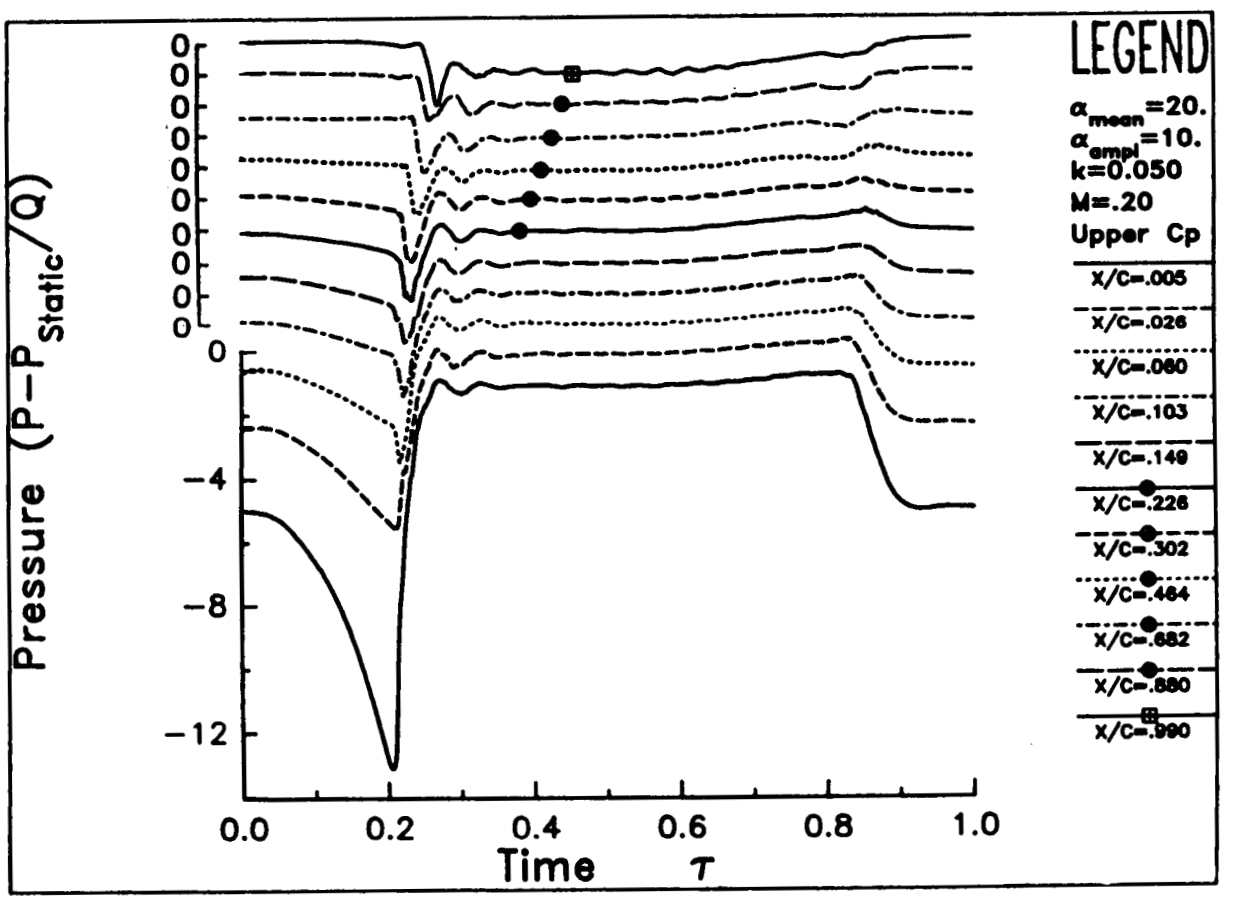

C-4

UNSTEADY PRESSURES, LOWER SURFACE, SINUSOID

The lower surface pressures for this same sinusoid are remarkable in that the maximum pressure change occurs at the trailing edge (to match the stalled suction surface pressure level), exhibits an initially damped behavior, and then stablilizes into a coherent vortex street response. The latter is noteworthy because in this ensemble-averaged data set the vortex street frequency must be synchronized with the fundamental frequency of the sinusoid. No single records were taken to permit close examination of the vortex street oscillation.

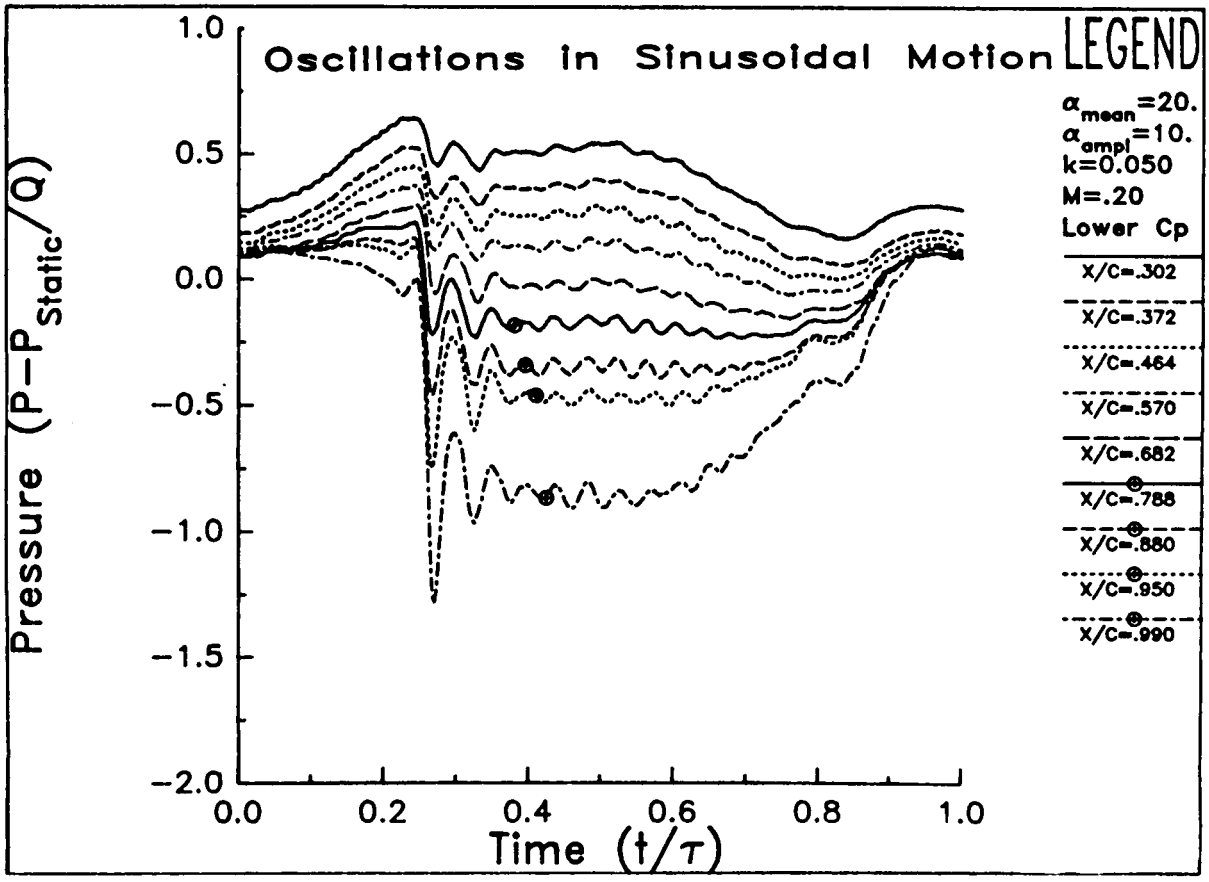

TRANSITION POINT DETECTION

Accurate determination of the point of boundary-layer transition is critical to many numerical computations. Surface heat transfer gages are usually required to determine the unsteady motion of the transition point. These gages are generally cumbersome to install and each requires a dedicated active anemometer circuit to operate. The techniques developed during the course of this study show that it may be possible to locate the transition point using the local increase in rms pressure measured by the unsteady pressure transducer as the local flow changes its character. An example of the correlation between the hot film and pressure transducer results is shown below. All results are at x/c = 0.026 for a 0 to 30 deg ramp at A = 0.02 and M = 0.20. The vertical pressure scale has been severely foreshortened, and only a small portion of the time scale is displayed. The increase in pressure rms corresponds to the increase in ensemble averaged heat transfer (upper curve) and to the spike in the rms heat transfer (second curve). No change at transition can be discerned in the ensemble-averaged pressure (bottom curve). If these promising early results are confirmed by additional correlations, this method may make it easier to locate transition in complex three-dimensional and unsteady flows.

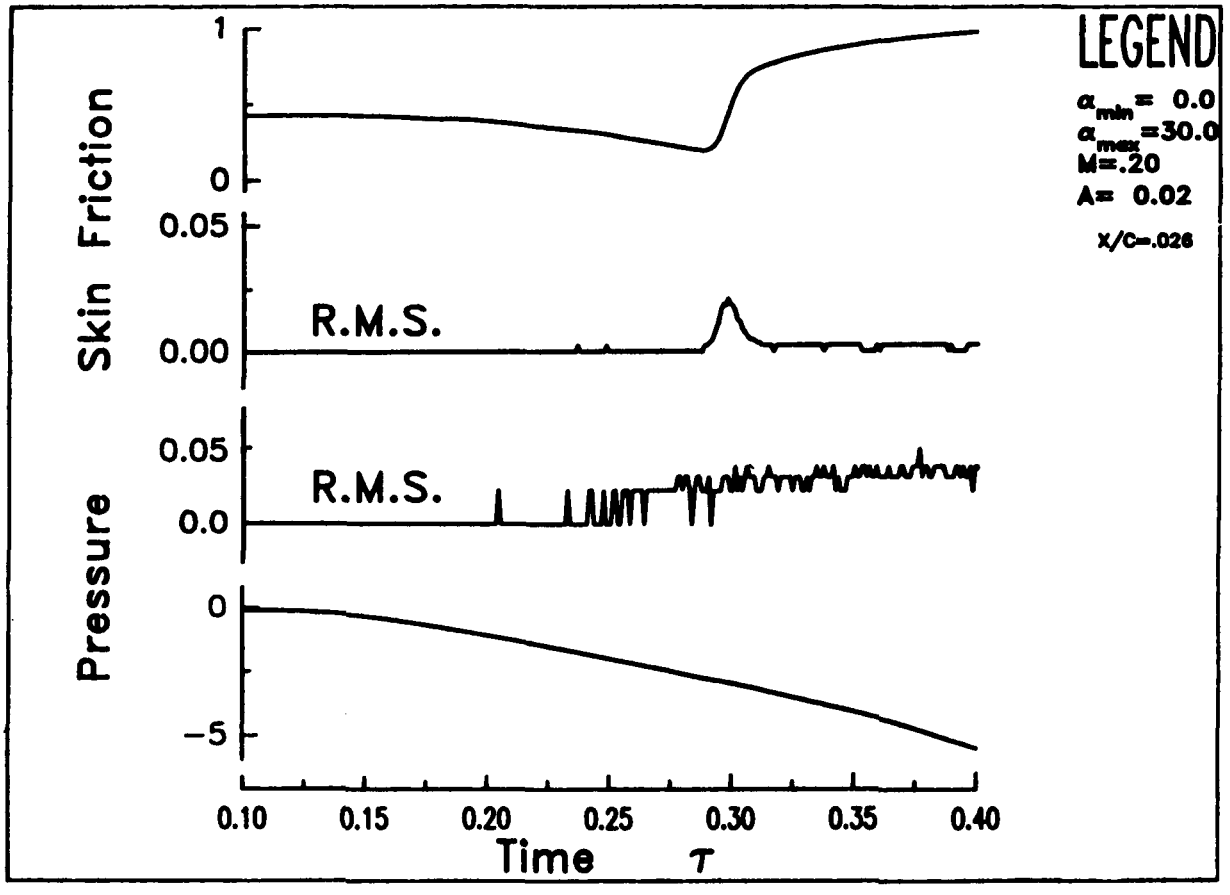

NOMENCLATURE

A	pitch rate, $\dot{\alpha}c/2U$, rad/sec
c	airfoil chord, m
C_D	section pressure drag coefficient, D/Qc
C_L	section lift coefficient, L/Qc
C_M	section pitching moment coefficient about x/c = 0.25, m/Qc^2
C_p	pressure coefficient, (P-Pstatic)/Q
k	reduced frequency of sinusoidal motion, $\omega c/2U$
Q	freestream dynamic pressure, $0.5\ \rho U^2$, Pa
t	time from start of data acquisition, sec
T	data acquisition period, sec
Re	Reynolds number, $c\ U/\nu$
U	freestream velocity, m/sec
x	distance from airfoil leading edge, m
α	geometric pitch angle, deg
ν	kinematic viscosity, m^2/sec
ρ	air density, kg/m^3
τ	nondimensional time, t/T
ω	frequency of sinusoidal oscillation, $2\pi f$

CONCLUSIONS

Conclusions - Increased Pitch Rate

- Stall events are delayed
- Stall vortex is strengthened
- Vortex propagation speed increases
- Unsteady airloads increase

Conclusions - M = 0.3, 0.4

- Supersonic zone near leading edge
- Stall vortex is weaker
- Unsteady airloads are reduced

Additional Conclusion

- Post stall vortex shedding when $Re_{bluff} < 10^6$
- Shedding synchronized when $A > 0.01$
- Sinusoids and ramps qualitatively similar

Note: This work was supported by the U.S. Air Force Office of Scientific Research under Contract F49620-84-0082 and will be reported in Ref. 11.

REFERENCES

1. Daley, D. C. and Jumper, E. J., "Experimental Investigation of Dynamic Stall for a Pitching Airfoil," Journal of Aircraft, Vol. 21, Oct. 1984, pp. 831-832.

2. Jumper, E. J., Schreck, S. J., and Dimmick, R. L., "Lift-Curve Characteristics for an Airfoil Pitching at Constant Rate," AIAA Paper 86-0117, Jan. 1986.

3. Walker, J. M., Helin, H. E., and Strickland, J. H., "An Experimental Investigation of an Airfoil Undergoing Large Amplitude Pitching Motions," AIAA Journal, Vol. 23, Aug. 1985, pp. 1141-1142.

4. Francis, M. S. and Keese, J. E., "Airfoil Dynamic Stall Performance with Large Amplitude Motions," AIAA Journal, Vol. 23, Nov. 1985, pp. 1653-1659.

5. Strickland, J. H. and Graham, G. M., "Force Coefficients for a NACA 0015 Airfoil Undergoing Constant Pitch Rate Motions," AIAA Journal, Vol. 25, April 1987, pp. 622-624.

6. Herbst, W. B., "Supermaneuverability," Proceedings of the AFOSR-FJSRL-University of Colorado Workshop on Unsteady Separated Flows, U.S. Air Force Academy, Colorado Springs, Aug. 1983.

7. Schlichting, H., "Boundary Layer Theory," McGraw-Hill, New York, 1979, pp. 31-32.

8. St. Hilaire, A. O. and Carta, F. O., "Analysis of Unswept and Swept Wing Chordwise Pressure Data from an Oscillating NACA 0012 Airfoil Experiment. Volume 1 - Technical Report," NASA CR-3567, March 1983.

9. Bisplinghoff, R. L. and Ashley, H., "Principles of Aeroelasticity," John Wiley and Sons, New York, 1962, pp. 120.

10. Gormont, R. E., "A Mathematical Model of Unsteady Aerodynamics and Radial Flow for Applications to Helicopter Rotors," USAAMRDL Technical Report 72-67, May 1973.

11. Lorber, P. F. and Carta, F. O., "Unsteady Stall Penetration Experiments at High Reynolds Number," United Technologies Research Center Report R87-956939-3, April 1987 (to be released as a technical report by the U.S. Air Force Office of Scientific Research).